Miniaturized Fully Passive Wireless Neural Recording With Heterogeneous Integration in Thin Packages

Sk Yeahia Been Sayeed, Satheesh Bojja Venkatakrishnan, *Senior Member, IEEE*, John L. Volakis, *Life Fellow, IEEE*, and Pulugurtha Markondeya Raj

***Abstract*— Wireless fully passive neural recording systems are demonstrated with heterogeneous integration of sensing, mixing, and communication components in flexible polymer dielectric films. The recording neurosensor has an antenna, antiparallel diode, and a bypass capacitor to modulate an incoming carrier signal with the neuropotentials and backscatter the mixed signal to an external reader circuit. Planar antennas are realized on liquid crystal polymer (LCP) flexible substrates with low dielectric constant. The designed antenna topology is realized with a single metal layer and eliminates the dependency on substrate thickness, and leads to thinner sensors. This is a major advance compared to prior passive neural recording with rigid and thicker substrates and components. Approximately, 80% thickness reduction and 20% volume reduction are achieved with a similar performance when compared to earlier studies. Our approach thus leads to low-cost and disposable wireless neurosensors on a flexible platform with heterogeneous integration. This article thus advances innovative wireless neural recording in three aspects: 1)advanced packaging for miniaturized neural recording with passive telemetry, through which the overall size of the sensor is reduced without degrading the performance; 2) new antenna topologies for neural recording applications; and 3) detailed power link analysis to estimate the minimum signal sensitivity.**

***Index Terms*— Heterogenous integration, liquid crystal polymer (LCP), miniaturization, wireless fully passive neurosensory, wireless neural recording.**

I. Introduction

EVER-INCREASING demand for medical devices has been fueling vital innovations in package integration of flexible bioelectronics for diagnostic and therapeutic systems. Medical device packaging can be classified into multiple categories depending on their use in either implantable or on-skin wearable environments. Rigid components on thick circuit boards in hermetic packages with feedthroughs and connectors are most common for implantable medical systems. Encapsulated rigid packaged devices on flexible carriers, embedding thin bare chips in flexible substrates, fabric-integrated electronics, and transferrable electronics as on-skin e-tattoos, form the key classes for wearable electronics. In all these classes of medical device packaging, there is a continual paradigm shift from rigid packages to thin, flexible packages while still meeting the demand for seamless power and data connectivity, and sensor integration for health monitoring. This shift is to enhance the user's comfort in terms of skin conformity, minimal obtrusiveness, and invasiveness and also avoid the need for frequent replacement. Additionally, to facilitate easier surgical implantation and less inflammation in the human body, miniaturized flexible packaged devices are preferred for implantable devices. To achieve the system functionality in such thin and flexible packages, it is necessary to integrate power and data telemetry, signal conditioning, and wireless communication functions with thin, flexible, and embedded components. High-density circuitry with advanced component integration in flexible substrates is the gateway to realizing this technology evolution.

Neural recording systems sense and communicate action or field potentials for several applications such as identification of pathological conditions and motor intent, and use the biofeedback to drive therapeutic or functional neurostimulation systems. They are fabricated at different scales depending on the electrode or channel count for the intended function, data rates or bandwidth, and power budget. For systems that record from 32, 64, or 100 channels, the data rates exceed 50 Mb/s and the power requirements exceed 100 mW, leading to energy consumption of 0.1–2 nJ/bit. One common way to design such wireless neural recording systems is to have them head-mount on the top of the skull. In this scenario, the rigid package with communication front-end, analog front-end signal modulation, and the battery is assembled on PCB substrates and encased in hermetic packages with feedthroughs that interface with electrodes. The size of the system can be as high as 100 cc. For example, a system of 51 × 38 x 38 mm^3 was designed with a power consumption is 63.2 mW, in which 28 mW is consumed by the RF transmitter [1]. A 1120 mA-h battery

Manuscript received 30 October 2022; accepted 3 March 2023. Date of publication 8 March 2023; date of current version 4 May 2023. Recommended for publication by Associate Editor S. Roy upon evaluation of reviewers' comments. *(Corresponding author: Sk Yeahia Been Sayeed.)*

Sk Yeahia Been Sayeed is with the Advanced Energy, Inc., Fort Collins, CO 80525 USA (e-mail: sbeen002@fiu.edu).

Satheesh Bojja Venkatakrishnan and John L. Volakis are with the Department of Electrical and Computer Engineering, College of Engineering and Computing, Florida International University, Miami, FL 33174 USA.

Pulugurtha Markondeya Raj is with the Department of Biomedical Engineering and the Department of Electrical and Computer Engineering, College of Engineering and Computing, Florida International University, Miami, FL 33174 USA.

Color versions of one or more figures in this article are available at https://doi.org/10.1109/TCPMT.2023.3253844.

Digital Object Identifier 10.1109/TCPMT.2023.3253844

operates for 2.9 days in this case. To avoid replacing battery, a rechargeable battery with wireless telemetry is implemented. For example, a head-stage neural recording system with 56 × 42 × 9 mm^3 was realized on a rigid package with a rechargeable battery [2]. The preamplifier and controller consume about 6 and 1 mW, respectively. Inductive charging becomes critical for communications with frequency shift key (FSK) that consumes ∼100 mW at Mb/s data rates. When the battery is charging, the average power can increase to 100 s of mW. Even though the system is powered by inductive coils, it has several issues. Overall power consumption is 350 mW, which is high enough that it may negatively affect the tissue, as it is well documented that more than 40 mW/cm^2 power dissipation raises the tissue temperature by more than 2 °C. Another way to design a neural recording system is in the form of subcutaneous microsystem. Such a system also has a recording unit and an external interrogator like the ones used in cortical recording. Implanted device has integrated circuit (IC) connected with probes, and the external device contains an antenna for data telemetry and inductive coil for power telemetry. Power consumption in such a scenario is less than 30 mW [3]. Since battery has limited lifetime, researchers have pursued ultralow-power IC technology to bypass the limited lifetime issue of battery and the associated safety and hazard issue. In such cases, custom-designed 32 channels, low-power ICs, and logic controller are used. Moreover, the whole system is on a rigid PCB, which is not mechanically compatible with the brain tissue and has a higher probability to create inflammatory responses that prevent safe and long-term use [4]. To reduce power consumption, researchers implemented multichannel electrode array with a uniquely designed low-power IC that is co-packaged with microfabricated traces and electrodes on Parylene C. IC is powered by an inductive coil at 300 MHz. The total size of the sensor is 6.5 × 6.5 mm and consumes 0.22 mW for 64 channels. Wireless communication is through backscattering. The packaged devices are assembled on a rigid PCB with solder to form the system interconnections [5].

The other class of neural recording systems comprises distributed individual untethered units that record from a single or few sites. These can be miniaturized to mm-scale, unlike the other units that are of 10–100 cc, and are also referred to as recording nodes or motes. These nodes are interrogated through new innovative transduction mechanisms and provide several unique opportunities for simplifying neural recording. Examples of such transduction include ultrasonic, RF, magnetoelectric, or multiferroic excitations. These multiphysics-based transduction techniques effectively reduce the size of the communication module and its power consumption. Ultrasonic energy is utilized to realize a small, tiny single channel neural recording device, which is sometimes referred to as neural dust. This device includes a piezoelectrical crystal and a transistor. An external transducer is used to communicate with the implanted neural dust. This technology has an edge over RF telemetry as ultrasound energy does not attenuate as much as RF energy in the tissue. Furthermore, because of the smaller wave propagation speeds of ultrasonic waves, the wavelengths are correspondingly smaller, thereby resulting in mm-scale transducers. A typical footprint of the sensor is 0.8 × 3 × 1 mm. However, a major drawback of the system is that ultrasound energy cannot penetrate efficiently through the skull [6]. RF backscattering technique is utilized to realize fully passive and implantable neural recording devices. In such systems, an antiparallel diode, a bypass capacitor, and a matching network are integrated together on a PCB substrate. The whole wireless neurosensor is designed to a size of 15 ×16 ×1.5 mm. With further advances in design, the device is miniaturized to 10 × 9 × 2.2 mm [7], [8]. Existing neuropotential sensors are based on rigid or flexible PCB substrates. In either scenario, bulky prep-packaged dies are used, and rigid soldering or anisotropic conductive paste (ACP) is implemented to interconnect the package and dies. Therefore, current sensors are based on thick modules.

In this study, a miniaturized flexible single-layer passive neuropotential sensor (9.5 × 8.7 × 0.5 mm) is demonstrated. Liquid crystal polymer (LCP) substrate is used as the flexible carrier for the circuit. A miniaturized spiral planar antenna is co-integrated with an antiparallel diode mixer and a bypass capacitor on the thin-flex LCP substrate with heterogeneous integration. The entire sensor is covered with biocompatible PDMS, leading to thin and flexible neural recording units for potential use in both on-skin and implantable applications.

II. Neurosensor Circuit Simulation and Fabrication

Neural recording system comprises two subsystems: 1) an implanted sensor and 2) an interrogator, as shown in Fig. 1. The external device or interrogator transmits a wireless 2.4 GHz carrier to the implanted transponder. After receiving the carrier signal, implanted sensor mixes the 2.4 GHz signal with low-frequency neural signals to produce the second harmonic at 4.8 GHz ± f_{neuro}. The modulated signal is then sent back to the external device or interrogator. Eventually, 4.8 GHz ± f_{neuro} can be observed or viewed at the spectrum analyzer (frequency domain) or demodulated to the original time-domain signal representing f_{neuro}. The implanted sensor (or neural recorder) composes of two components: 1) passive mixer circuit and 2) wireless telemetry. An RF antenna operating at 2.4 and 4.8 GHz acts as the wireless telemetry interface, and the mixer modulates neural signal (f_{neuro}) and backscatters (4.8 GHz ± f_{neuro}) to the interrogator or an external device via the antenna in the implanted sensor.

One of the challenges in implanted neurosensors is to decrease the antenna size to achieve minimally invasiveness. Several miniaturization techniques have been developed. These include: 1) Stacked multiple radiating patches on top of each other [9], [10]; 2) Planar-inverted F antenna configuration [11], [12], [13]; 3) Capacitive, inductive, or split-ring loading to match impedance [14], [15], [16]; 4) Increased current path by meandering or spiraling [17], [18], [19], [20]; and 5) Antennas on substrates with high dielectric constant [21], [22]. Although these techniques document antennas

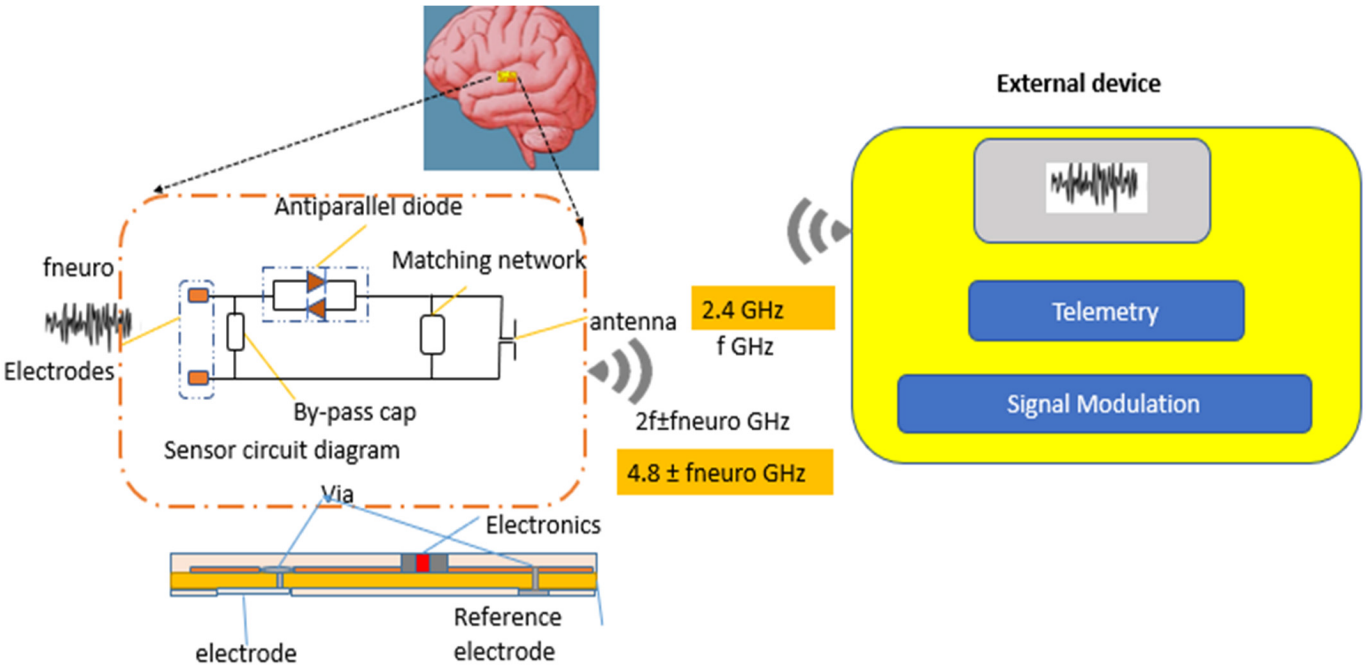

Fig. 1. Neural recording system: sensor circuit diagram with APDP, antenna, and bypass capacitor. Interrogating signal 2.4 GHz is sent to the implanted sensor, f_{neuro} comes from the brain and the mixer circuit yields (4.8 GHz $\pm$ f_{neuro}). The up-converted signal is sent back to the external circuitry.

with small footprint and good radiation performance, higher thickness has always been a major drawback. Since our application requires thinness, flexibility, and biocompatibility, these telemetries fall short in meeting the requirements. Recent work reported antennas on flexible substrates with low dielectric constant. However, their footprints are generally larger. To remove the substrate thickness, various coplanar antenna topologies are also investigated. In our work, to meet the flexibility, stability, and thinness requirements along with resistance to moisture, we chose LCP with a coplanar spiral structure to shrink the antenna size. Such a structure was first shown in [23], however, with a single band. Our approach advances this further to achieve a broad dual-band (2.4 and 4.8 GHz) performance.

This antenna-in-package approach also co-integrates the antenna with passive circuitry to realize a miniaturized neural sensor. The neural sensor's schematic circuit is shown in Fig. 1. The planar antenna was designed on Rogers 3850HT substrates with permittivity of 2.9 and loss tangent of 0.002. A subharmonic mixer is operated with a local oscillator (LO) at half of the typical conventional mixer's LO frequency. It yields the $2f_{\text{LO}} \pm f_{\text{neuro}}$ signal with f_{LO}, while conventional mixers generate the same output with $2f_{\text{LO}}$. The subharmonic mixer circuit's components are an antiparallel diode pair (APDP), a matching circuit, a bypass capacitor, and a pair of electrodes. An APDP (Si MA4E2508L-1112) and matching network with transmission line and discrete bypass capacitors (7.5 pF) were integrated with the antenna to accomplish the complete design of the neural sensor.

Estimation of the overall system performance metrics, such as total end-to-end chain loss and backscattered power with the passive circuit requires detailed circuit simulations. The circuit comprises an external antenna and implanted antenna, diode, and capacitors. Cadence[1] AWR Design Environment[1] was used to simulate the whole neurosensor and predicts the backscattered power. A matching network is required to match the antenna and the APDP impedance. The role of bypass capacitor is to shunt the 2.4 GHz wireless link. APDP performance metrics from vendor datasheets were input into the model. An ac signal source at an amplitude of 1 mV_{pp} and frequency of 1 kHz (f_{neuro}) was used to mimic the neuropotential. For an input power of 15 dBm, the backscattered signal (4.8 GHz $\pm$ 1 kHz) power is approximately -105 dBm for the modulated neural signal, which is well above the sensitivity of the signal analyzer -120 dBm. The simulated circuit performance with sideband performance is shown in Fig. 2. To detect the neurosignal, the backscattered power has to be 5 dB above the signal analyzer sensitivity.

As described before, Rogers 3850 HT was used as the substrate because of its excellent properties at high frequencies, good dimensional stability, and low moisture absorption rate. The fabrication process is illustrated in Fig. 3. Subtractive copper patterning with dry-film photoresist sensors was performed to acquire the desired line definition and high conductivity for sensor traces in contrast to printed silver traces. Dry-film photoresist (Hitachi Chemicals, RY-5115[1]) was utilized to eventually support large-area fabrication at low cost. The process starts with substrate cleaning and micro etching to enhance adhesion during photoresist patterning and copper etching. UV light was used for lithography at 360 nm narrowband wavelength with an energy dose of 100–120 mJ/cm^2. The photoresist pattern for the copper trace

[1]Registered trademark.

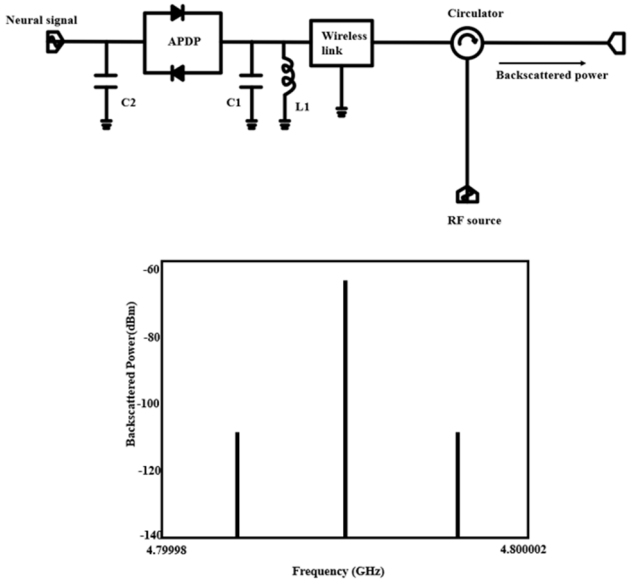

Fig. 2. Complete circuit model of neurosensor (top). Backscattered sideband power is shown in the frequency domain. The predicted power level is −105 dBm (bottom). Path 2 loss is 47 dB.

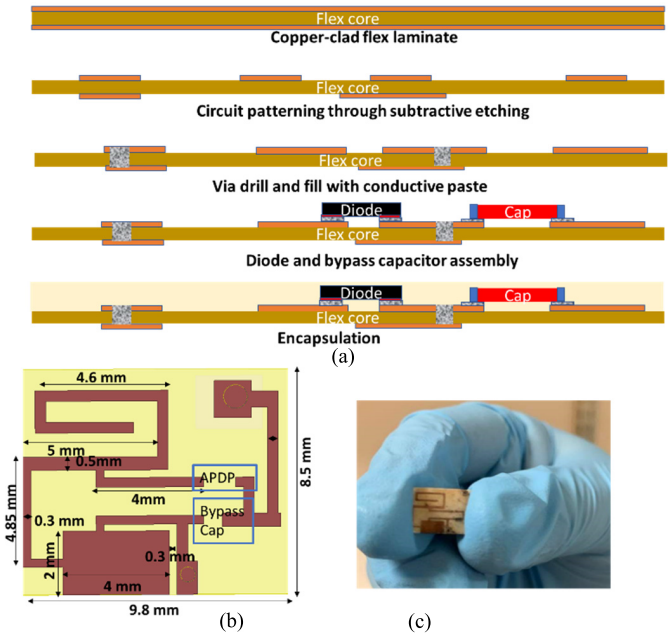

Fig. 3. (a) Device fabrication process and assembly. (b) Layout and geometry of the neurosensor. (c) Optical photograph of the fabricated neurosensor.

circuit was then developed in a 1% sodium borate solution at 60 °C for 65 s, followed by rinsing in DI water. To improve the etching rate, the etchant was heated to 60 °C. In the end, photoresist was removed with acetone to expose the copper traces. The substrate was subsequently laser-drilled with vias to interface with the electrodes on the backside. Silver loading with an ink content of 65% was used to fill the vias with a vacuum-assisted via-filling machine. The via electrical connectivity was tested with a multimeter. Compared to silver pastes with 85% particle loading, lower loading of 65% showed better mechanical strength and lower contact resistance. Conductive silver elastomer adhesive as chip-to-flex interconnection layers was utilized for surface assembly of devices to enhance electrical and reliability performance. For biocompatibility, the whole sensor was encapsulated with a PDMS coating.

III. Result and Discussion

A. Electrical Characterization Results

The measurement set-up for evaluating the prototype is shown in Fig. 4. A LO signal was generated by a signal generator. The transmitted power was set at 15 dBm, which is well below the APDP's absolute maximum (20 dBm), and provided to the external interrogating antenna through a circulator. An arbitrary function generator was used for creating the emulated neurosignal $f_{\text{neuro}} = 1$ kHz with a magnitude of 1 mV_{pp}. The neurorecording device was positioned inside the brain phantom. The phantom consists of skin, bone, dura/gray, and white matter. Recipe of the phantom was taken from prior work [7]. A spectrum analyzer was used to detect the received signal (4.8 GHz $\pm$ f_{neuro}) at the reader side, as shown in Fig. 4. Measured spectral response is also shown in the figure. For an input power of 15 dBm, the backscattered sideband RF power is measured as −109 dBm while the emulated neural signal is at 1 mV_{pp} or −58 dBm. Overall system loss was 51 dB, which is reasonable to detect neural signal 1 mV_{pp} at 1 kHz while the implantable and external antennas are 17 mm apart, as illustrated by Fig. 4(b). The discrepancy between the measured value of −109 dBm and the simulated value of the sideband power of −105 dBm from Fig. 2 is 4 dB. This difference between the simulation and measurement results is mainly because of fabrication and additional unaccounted parasitic values. When implantable neural sensors are placed under the skin and the interrogator is 2 mm away, the system loss is 31 dB, deduced as the difference between the input neural power of −58 dBm and the received sideband power of −89 dBm, as illustrated in Fig. 5, which is similar to the values reported in [8]. Fig. 6 (Bottom) indicates that the Path 2 loss for 5 dBm of incoming RF power is ∼27 dB when the sensor and interrogator are 2 mm apart and the sensor is under the skin, again showing 4 dB discrepancy from simulations. This analysis is further discussed below.

B. System Performance Analysis and Projection

The key performance metrics for a neural recording unit are: 1) low interrogating power; 2) high backscattering power because of low conversion, propagation, and other system losses; and 3) high sensitivity to weak (20 μV) neurosignals. These three aspects are examined in detail here with a simple diagram Fig. 6 (Top).

The Path 1 loss is guided by two factors, viz., propagation loss at 2.4 GHz and matching loss. The incoming power should compensate for the propagation losses from the interrogator to the device through the air and tissue and losses from the mismatch

$$\text{Path 1 loss} = L_{\text{Propag@2.4 GHz}}[\text{dB}] + L_{\text{Match}}\ [\text{dB}]. \quad (1)$$

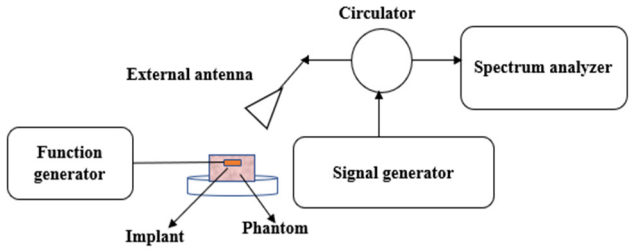

(a)

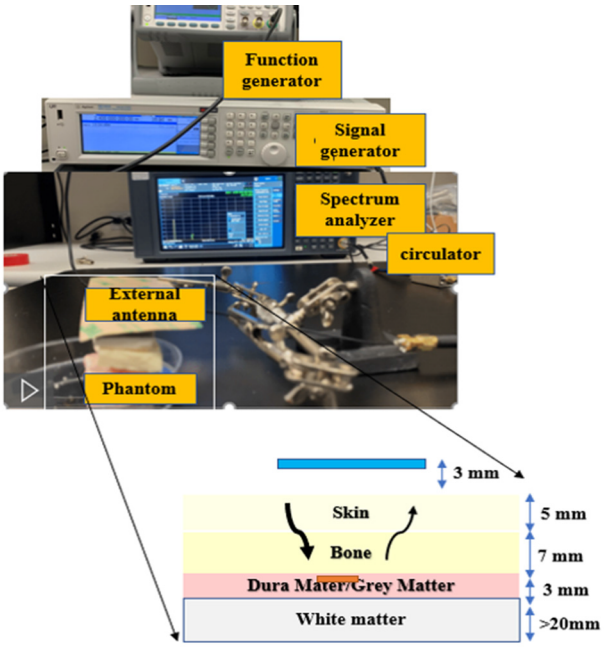

(b)

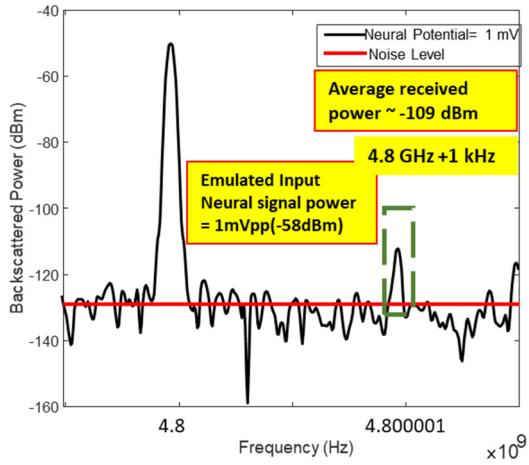

(c)

Fig. 4. (a) Block diagram of the sensor and receiving system. (b) Experimental setup for characterizing the neurosensory. (c) Frequency domain performance of the sensor. Emulated neural voltage is 1 mV_{pp} and frequency is 1 kHz. Average received power is −109 dBm. External antenna and sensor are 17 mm away in this case. Path 2 loss is 51 dB.

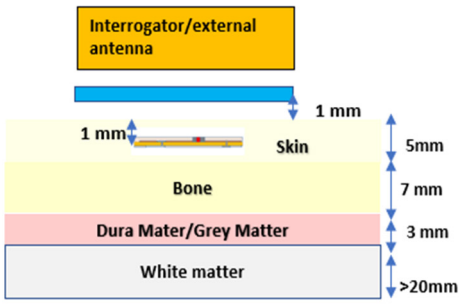

(a)

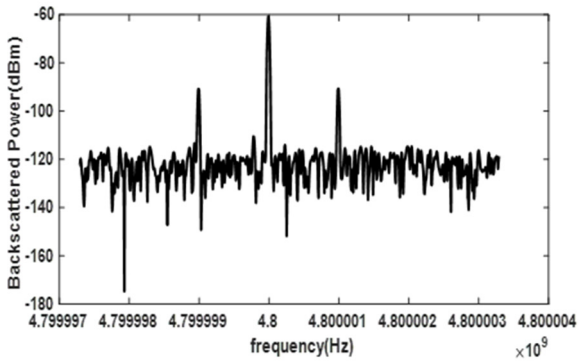

(b)

Fig. 5. (a) Position of the interrogator antenna from implantable neural recording sensor. They are 2 mm apart in this specific case. (b) Frequency-domain spectrum shows that the backscattered power is at −89 dBm. Path 2 loss is 31 dB.

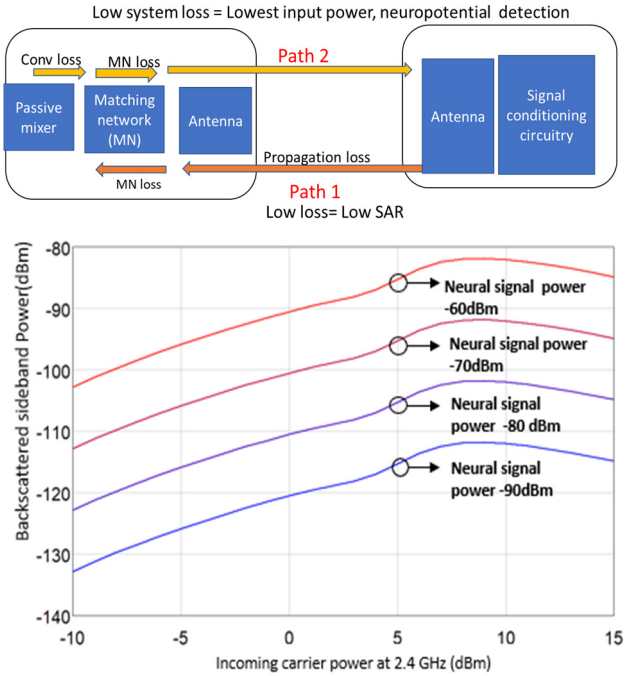

Fig. 6. System loss includes conversion loss, matching network loss, and propagation loss (top). Backscattered sideband power as a function of the power of the incoming carrier (2.4 GHz) power at various neural signal power levels (bottom).

We will focus on Path 2 loss, which is also interpreted as system loss in this work because it results in lower recorded neuropotential signal power. The system loss in Path 2 is related to the conversion loss, matching, and propagation losses, as shown in Fig. 6 (top) and described in (2). System

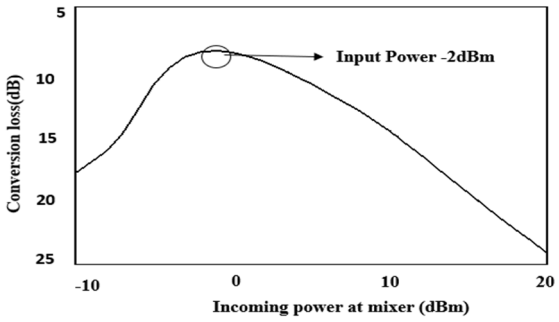

Fig. 7. Incoming power at mixer versus conversion loss. Optimized input power is −2 dBm and corresponding conversion loss is 9 dB.

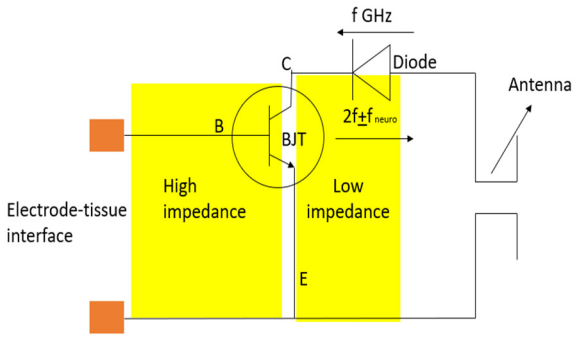

Fig. 8. Novel passive neural recording sensor with a simple BJT and diode. BJT changes the high impedance into low impedance.

loss can be represented as

$$\begin{aligned}\text{System loss in Path 2 [dB]} &= L_{\text{Conversion loss@4.8GHz}\pm f\text{neuro}}\ \text{[dB]} \\ &+ L_{\text{Propag@4.8GHz}\pm f\text{neuro}}\ \text{[dB]} \\ &+ L_{\text{Match}}\ \text{[dB]}. \end{aligned} \tag{2}$$

$L_{\text{Conversion loss}}$ is the loss during the conversion from input carrier power to the backscattered carrier signal power, $L_{\text{Propag@4.8 GHz}\pm f\text{neuro}}$ is the propagation loss at 4.8 GHz $\pm$ f_{neuro}, and L_{Match} is the mismatch loss between implanted antenna and APDP. The conversion loss is lowest (9 dB) when the input power at the mixer without any path loss is −2 dBm. As the power deviates from the optimal value, the losses increase. The plot of the conversion loss as a function of the incoming power was simulated and estimated, as shown in Fig. 7, for the completion of the discussion.

Tissue behaves as a conductor at high frequencies as the human body becomes a medium with high-dielectric loss. As the backscattered RF signal propagates from a high-dielectric-constant medium to a low-dielectric-constant medium, it bends away from the direction perpendicular to the interface. In other words, the signal effectively travels longer distances in an inhomogeneous tissue and also encounters multiple reflections. With higher propagation loss, the transmitter needs to transmit at higher power to keep the conversion loss under control so that a higher signal sensitivity is achieved. Therefore, placing the implantable neural sensor just under the skin [Fig. 4(b)] would decrease the propagation loss and lead to a lower power carried by the incoming carrier at 2.4 GHz. One other way to avoid this high propagation loss is to introduce multiferroic antennas [24] that operate at lower frequencies.

The key system metric is the sideband neural signal power that can be detected by the receiver circuit. The lowest neural signal that can be detected is dependent on minimum receiver sensitivity and system loss. With low system loss, we can record weaker neuropotential signals. Subtracting the lowest detectable neural signal power from minimum receiver sensitivity yields tolerable system loss, as described by the following:

$$\begin{aligned}&\text{Lowest Neuropotential [dBm]} \\ &\quad = \text{Minimum of the receiver sensitivity} \\ &\quad + \text{System loss in Path 2.}\end{aligned} \tag{3}$$

From the analysis, the backscattered power should be at least −125 dBm so that the carrier power at the receiver is adequate and above −130 dBm. For this receiver sensitivity of −130 dBm, the lowest neuropotential signal is −90 dBm (20 μV), when the target system loss is 35 dB. In other words, as long as the sum of conversion modulation loss, matching loss, and propagation loss at 4.8 GHz is less than 35 dB, we can detect neuropotential signals as low as 20 μV. Reducing the distance between the implant and sensor leads to a decrease in propagation loss. When fixing the distance between external antenna and implantable sensor to 2 mm, we predict that 20 μV can be acquired with the optimal incoming power at 2.4 GHz power because the measured Path 2 loss for 2 mm is only 31 dB. As seen from the equation, it is critical to minimize both the propagation and mixing losses to achieve superior signal sensitivity.

Additional mixing losses arise from the APDP and the impedance mismatch between the incoming neural signal and the APDP. For example, the electrodes are at high impedance, which invariably leads to substantial losses in the signal that the APDP receives at its input. Impedance-matched recording is hence preferred to lower these losses. One way to achieve this is by utilizing electrodes with higher surface area and closer to the neural signal source. Impedance transformation with a bipolar junction transistor (BJT) device is also an alternative approach to address this challenge [6]. We will briefly discuss this novel circuit topology shown in Fig. 8. In this approach, the diode not only acts as a dc bias for BJT but also as a mixer, while the BJT converts the high impedance coming from the electrode-tissue interface into low impedance, resulting in recording low-potential brain signals [25]. However, small form factor with bare die PNP BJT and diode with embedded packaging is yet to be realized.

Specific absorption rate (SAR) is an estimate of the RF energy absorbed by the human body or tissue while a wireless transmission occurs. The SAR generated by our neurosensing system was assessed by ANSYS[1]HFSS. The implant was 1 mm below the skin layer, and the external antenna was 1 mm above the skin layer, as shown in Fig. 5(a). An RF input power of 5 dBm is assumed at 2.4 GHz. The calculated $\text{SAR}_{1\,\text{g}}$ is 0.97 W/kg while $\text{SAR}_{10\,\text{g}}$ is 0.13 W/kg, which are in compliance with Federal Communications Commission (FCC) for uncontrolled environment exposure ($\text{SAR}_{1\,\text{g}} < 1.6$ W/kg)

TABLE I
COMPARISON OF PRIOR PACKAGE INTEGRATION STRATEGY AND THE SIZE OF NEURAL RECORDING DEVICES WITH OUR WORK

	Size	Packaging
[1]	$51 \times 38 \times 38$ mm^3	Rigid substrate, thick prepacked dies, and rigid soldering for interconnections
[2]	$56 \times 42 \times 9$ mm^3	
[7,8]	$10 \times 9 \times 2.2$ mm^3	
Our work	$9.5 \times 8.7 \times 0.5$ mm^3	Flexible substrate, thin chip, and silver elastomer for interconnection

[26] and International Commission on Non-Ionizing Radiation Protection (ICNIRP) ($SAR_{10\,g} < 2$ W/kg) [27], respectively. Therefore, our neurosensing system is projected to meet the patient safety guidelines.

C. Package Size Analysis

The package size is determined by the antenna footprint, mixer, matching components and interconnects. This size is usually much smaller than the electrode extensions between the neurosensor and the neural interfaces. Since the electrode design is customized to the target recording application and is not a key focus of this work, and we only compare the neurosensor size without including the electrode size. The size or form factor of previous rigid packages on circuit boards is compared with current packages in this work in Table I. This work implements planar antennas on flexible substrates. The proposed monopole spiral antenna is agnostic to the substrate thickness, making it much thinner than today's neurosensor devices. As the telemetry is substrate thickness-independent, the neural recording system can be implemented on much thinner substrates (for example, 50 μm thick flexible substrate). Comparing to other published work, our work thus demonstrates thinner, smaller, and flexible packages due to planar antenna design, single-layer circuitry, and thin chips.

The next key factor that determines the module thickness is the component thickness and off-chip interconnection height. In traditional packaging, electronic components are assembled onto the substrate with thick solder joints at temperatures above 230 °C and encapsulated, which eventually lead to thicker packages. Moreover, prepackaged thicker chips in leadframe Quad Flat No-Lead (QFN) packages lead to bulky packages. To realize thinner substrates, it is necessary to embed electronic components into the flexible substrate. This is consistent with the emerging trend of sub-100 μm dies for embedding and fan-out packaging technologies. In fan-out packaging with chip-embedding in flexible carriers, substrates with cavities and a back-up layer are fabricated as the first step. Devices are then assembled into the cavities, and off-chip interconnects are directly formed from the chip pads to the package traces with printed conductive elastomers. Additionally, a thinner die is connected with copper traces and silver-elastomer interconnects, which does not add any substantial height to the package. More importantly, advanced packaging with embedding dies and thin-film passive components in flex will further reduce the size of neurosensors. Such trends have been recently realized to further reduce the package form factor [28]. Passive electrode impedance matching in neural recording sensors, when realized with embedded packaging, will further reduce the system losses and increase the signal sensitivity.

IV. SUMMARY

Heterogeneous integration of thin active devices, power and data telemetry, and storage components in thin, flexible substrates will pave the way for miniaturized bioelectronics. Toward this goal, we have shown a passive telemetry communication system for transmitting neural signals. A simplified passive backscattering approach miniaturizes the topology and bill-of-materials for system components. Innovative topologies with monopole spiral miniaturized antennas further reduced the system size. Complete system loss analysis showed cumulative propagation losses of approximately 30 dB for the backscattered signals. The projected signal sensitivity for this system is 20 μV, assuming a receiver sensitivity of -130 dBm. With the decreasing distance between the interrogator antenna and the implanted sensor, the required input power is reduced to 5 dBm, which is adequate to acquire neuropotential as low as 20 μV. The lowest input power for the system function can be further reduced with advances in the diode or mixers. The article thus reports advances in package miniaturization, innovative telemetry topologies, and detailed power link analysis to predict the neural signal sensitivity.

REFERENCES

[1] C. A. Chestek et al., "HermesC: Low-power wireless neural recording system for freely moving primates," *IEEE Trans. Neural Syst. Rehabil. Eng.*, vol. 17, no. 4, pp. 330–338, Aug. 2009, doi: 10.1109/TNSRE.2009.2023293.

[2] D. A. Borton, M. Yin, J. Aceros, and A. Nurmikko, "An implantable wireless neural interface for recording cortical circuit dynamics in moving primates," *J. Neural Eng.*, vol. 10, no. 2, Apr. 2013, Art. no. 026010, doi: 10.1088/1741-2560/10/2/026010.

[3] K.-W. Cheng et al., "100-channel wireless neural recording system with 54-Mb/s data link and 40%-efficiency power link," in *Proc. IEEE Asian Solid State Circuits Conf. (A-SSCC)*, Dec. 2012, pp. 185–188, doi: 10.1109/IPEC.2012.6522656.

[4] C. Mestais, G. Charvet, F. Sauter-Starace, M. Foerster, D. Ratel, and A. L. Benabid, "WIMAGINE: Wireless 64-channel ECoG recording implant for long term clinical applications," *IEEE Trans. Neural Syst. Rehabil. Eng.*, vol. 23, no. 1, pp. 10–21, Jan. 2015, doi: 10.1109/TNSRE.2014.2333541.

[5] R. Müller et al., "A minimally invasive 64-channel wireless μECoG implant," *IEEE J. Solid-State Circuits*, vol. 50, no. 1, pp. 344–359, Jan. 2015, doi: 10.1109/JSSC.2014.2364824.

[6] D. Seo et al., "Wireless recording in the peripheral nervous system with ultrasonic neural dust," *Neuron*, vol. 91, no. 3, pp. 529–539, Apr. 2016, doi: 10.1016/J.NEURON.2016.06.034.

[7] A. Kiourti, C. W. L. Lee, J. Chae, and J. L. Volakis, "A wireless fully passive neural recording device for unobtrusive neuropotential monitoring," *IEEE Trans. Biomed. Eng.*, vol. 63, no. 1, pp. 131–137, Jan. 2016, doi: 10.1109/TBME.2015.2458583.

[8] C. Moncion, L. Balachandar, S. Bojja-Venkatakrishnan, J. J. Riera, and J. L. Volakis, "Fully-passive wireless implant for neuropotential acquisition: An in vivo validation," *IEEE J. Electromagn., RF Microw. Med. Biol.*, vol. 3, no. 3, pp. 199–205, Sep. 2019, doi: 10.1109/JERM.2019.2895657.

[9] C.-M. Lee, T.-C. Yo, and C.-H. Luo, "Compact broadband stacked implantable antenna for biotelemetry with medical devices," in *Proc. IEEE Annu. Wireless Microw. Technol. Conf.*, Dec. 2006, pp. 1–4, doi: 10.1109/WAMICON.2006.351945.

[10] W.-C. Liu, S.-H. Chen, and C.-M. Wu, "Implantable broadband circular stacked PIFA antenna for biotelemetry communication," *J. Electromagn. Waves Appl.*, vol. 22, no. 13, pp. 1791–1800, Jan. 2008, doi: 10.1163/156939308786375181.

[11] C. Liu, Y.-X. Guo, and S. Xiao, "Compact dual-band antenna for implantable devices," *IEEE Antennas Wireless Propag. Lett.*, vol. 11, pp. 1508–1511, 2012, doi: 10.1109/LAWP.2012.2233705.

[12] R. Warty, M. R. Tofighi, U. Kawoos, and A. Rosen, "Characterization of implantable antennas for intracranial pressure monitoring: Reflection by and transmission through a scalp phantom," *IEEE Trans. Microw. Theory Techn.*, vol. 56, no. 10, pp. 2366–2376, Oct. 2008, doi: 10.1109/TMTT.2008.2004254.

[13] J. Kim and Y. Rahmat-Samii, "Implanted antennas inside a human body: Simulations, designs, and characterizations," *IEEE Trans. Microw. Theory Techn.*, vol. 52, no. 8, pp. 1934–1943, Aug. 2004, doi: 10.1109/TMTT.2004.832018.

[14] C. Liu, Y.-X. Guo, and S. Xiao, "Capacitively loaded circularly polarized implantable patch antenna for ISM band biomedical applications," *IEEE Trans. Antennas Propag.*, vol. 62, no. 5, pp. 2407–2417, May 2014, doi: 10.1109/TAP.2014.2307341.

[15] L.-J. Xu, Y.-X. Guo, and W. Wu, "Bandwidth enhancement of an implantable antenna," *IEEE Antennas Wireless Propag. Lett.*, vol. 14, pp. 1510–1513, 2015, doi: 10.1109/LAWP.2014.2374217.

[16] L.-J. Xu, Y.-X. Guo, and W. Wu, "Miniaturized dual-band antenna for implantable wireless communications," *IEEE Antennas Wireless Propag. Lett.*, vol. 13, pp. 1160–1163, 2014, doi: 10.1109/LAWP.2014.2329937.

[17] L.-J. Xu, Y.-X. Guo, and W. Wu, "Dual-band implantable antenna with open-end slots on ground," *IEEE Antennas Wireless Propag. Lett.*, vol. 11, pp. 1564–1567, 2013, doi: 10.1109/LAWP.2012.2237010.

[18] I. Gani and H. Yoo, "Multi-band antenna system for skin implant," *IEEE Microw. Wireless Compon. Lett.*, vol. 26, no. 4, pp. 294–296, Apr. 2016, doi: 10.1109/LMWC.2016.2538470.

[19] C. Liu, Y.-X. Guo, and S. Xiao, "A hybrid patch/slot implantable antenna for biotelemetry devices," *IEEE Antennas Wireless Propag. Lett.*, vol. 11, pp. 1646–1649, 2012, doi: 10.1109/LAWP.2013.2237879.

[20] P. Soontornpipit, C. M. Furse, and Y. C. Chung, "Miniaturized biocompatible microstrip antenna using genetic algorithm," *IEEE Trans. Antennas Propag.*, vol. 53, no. 6, pp. 1939–1945, Jun. 2005, doi: 10.1109/TAP.2005.848461.

[21] A. Kiourti and K. S. Nikita, "Miniature scalp-implantable antennas for telemetry in the MICS and ism bands: Design, safety considerations and link budget analysis," *IEEE Trans. Antennas Propag.*, vol. 60, no. 8, pp. 3568–3575, Aug. 2012, doi: 10.1109/TAP.2012.2201078.

[22] A. Kiourti, M. Christopoulou, and K. S. Nikita, "Performance of a novel miniature antenna implanted in the human head for wireless biotelemetry," in *Proc. IEEE Int. Symp. Antennas Propag. (APSURSI)*, Jul. 2011, pp. 392–395, doi: 10.1109/APS.2011.5996726.

[23] M. W. A. Khan, E. Moradi, L. Sydänheimo, T. Björninen, Y. Rahmat-Samii, and L. Ukkonen, "Miniature coplanar implantable antenna on thin and flexible platform for fully wireless intracranial pressure monitoring system," *Int. J. Antennas Propag.*, vol. 2017, pp. 1–9, Jan. 2017, doi: 10.1155/2017/9161083.

[24] M. Zaeimbashi et al., "NanoNeuroRFID: A low loss brain implantable device based on magnetoelectric antenna," in *Proc. IEEE Int. Microw. Biomed. Conf. (IMBioC)*, Jun. 2018, pp. 205–207, doi: 10.1109/IMBIOC.2018.8428892.

[25] W.-C. Chen, K. Guido, and A. Kiourti, "Passive impedance matching for implanted brain–electrode interfaces," *IEEE J. Electromagn., RF Microw. Med. Biol.*, vol. 3, no. 4, pp. 233–239, Dec. 2019, doi: 10.1109/JERM.2019.2904024.

[26] R. F.-O. Bulletin and Undefined 1997. (2001). *Evaluating Compliance With FCC Guidelines for Human Exposure to Radiofrequency Electromagnetic Fields*. Accessed: Nov. 16, 2021. [Online]. Available: rfcec.com

[27] International Commission on Non-Ionizing Radiation Protection (ICNIRP). (1998). *Guidelines for Limiting Exposure to Time-Varying Electric, Magnetic and Electromagnetic Fields (up to 300 GHz)*. Health Physics. Accessed: Nov. 16, 2021. [Online]. Available: https://ci.nii.ac.jp/naid/10011773744

[28] S. Y. B. Sayeed, D. Wilding, J. S. Camara, D. Vital, S. Bhardwaj, and P. M. Raj, "Deformable interconnects with embedded devices in flexible fan-out packages," in *Proc. Int. Symp. Microelectron.*, vol. 2019, no. 1, Oct. 2019, Art. no. 000163, doi: 10.4071/2380-4505-2019.1.000163.

Sk Yeahia Been Sayeed received the B.Sc. degree in electrical, electronic, and communication engineering from the Military Institute of Science and Technology (MIST), Dhaka, Bangladesh, in 2015, and the Ph.D. degree from Florida International University, Miami, FL, USA, in 2022, focusing on bioelectronics, wireless neural recording sensors, and 3-D heterogeneous advanced flex packaging.

In fall of 2017, he joined the Department of Biomedical Engineering, Florida International University and started working with Dr. Pulugurtha Markondeya Raj, in 2019. He is currently working at Plasma Power in Advanced Energy, Inc., USA, as an Electronic Engineer. He has authored and coauthored 11 articles as of March 2023.

Dr. Been Sayeed received the Best Poster Award from the iMAPS Workshop in 2019.

Satheesh Bojja Venkatakrishnan (Senior Member, IEEE) was born in Tiruchirappalli, India, in 1987. He received the bachelor's degree in electronics and communication engineering from the National Institute of Technology, Tiruchirappalli, in 2009, and the M.S. and Ph.D. degrees in electrical engineering from The Ohio State University (OSU), Columbus, OH, USA, in 2017.

He was a Scientist with DRDO, India, from 2009 to 2013, working on the development and implementation of active electronic steerable antennas. He is currently an Assistant Professor with the Department of Electrical and Computer Engineering, Florida International University, Miami, FL, USA. His current research interests include RF system design for secure wideband communications, data sensing and imaging, interference mitigation techniques, and RFSoC-based Simultaneous Transmit and Receive System (STAR) to improve the spectral efficiency. In parallel, he has been working on developing RF sensors and circuits including fully passive neural implants and multi-modal patch sensors for biomedical applications.

Dr. Bojja Venkatakrishnan is a member of Phi Kappa Phi, and also an Associate Member of USNC–URSI. He has won numerous awards and recognitions including the IEEE Electromagnetic Theory Symposium (EMTS-2019) Young Scientist Award, and the Best Paper Award from the International Union of Radio Science General Assembly and Scientific Symposium (URSI-GASS) held at Montreal, Canada, in August 2017.

John L. Volakis (Life Fellow, IEEE) was born on May 13, 1956, in Chios, Greece, and immigrated to the USA, in 1973. He received the B.E. degree (summa cum laude) from Youngstown State University, Youngstown, OH, USA, in 1978, and the M.Sc. and Ph.D. degrees from Ohio State University, Columbus, OH, in 1979 and 1982, respectively.

He started his career at Rockwell International from 1982 to 1984, now Boeing. In 1984, he was appointed as an Assistant Professor at The University of Michigan, Ann Arbor, MI, USA, becoming a Full Professor, in 1994. He also served as the Director of the Radiation Laboratory from 1998 to 2000. From January 2003 to August 2017, he was the Roy and Lois Chope Chair Professor of Engineering at The Ohio State University and served as the Director of the ElectroScience Laboratory, from 2003 to 2016. Since August 2017, he has been the Dean of the College of Engineering and Computing and a Professor with the Department of Electrical and Computer Engineering, Florida International University (FIU), Miami, FL, USA. He is also the authors of nine books, including the *Antenna Handbook*, referred to as the "antenna bible." He has graduated/mentored 105 doctoral students/post-docs with 43 of them receiving best paper awards at conferences. He has published over 450 journal articles, over 950 conference papers, over 30 chapters, and over 30 patents/disclosures. Over the years, he has carried out pioneering research in electromagnetics (EM), RF materials and metamaterials, antennas and phased array, RF transceivers, textile electronics, millimeter waves and terahertz, EMI/EMC as well as EM diffraction and computational methods. His research team is recognized for introducing and/or developing 1) hybrid finite element methods for microwave engineering, now widely used in commercial RF design packages, 2) novel composite materials for antennas and sensor miniaturization, 3) a new class of wideband conformal antennas and arrays with over 30:1 of contiguous bandwidth, referred to as tightly coupled dipole antennas, 4) textile surfaces for wearable electronics and sensors, 5) batteryless and wireless medical implants for noninvasive brain signal collection, 6) diffraction coefficients for material coated edges, and for 7) model-scaled radar scattering verification methods.

Prof. Volakis is a fellow of AAAS, NAI, URSI, and ACES. He was listed by ISI among the top 250 most referenced authors in 2004. Among his awards are: The University of Michigan College of Engineering Research Excellence Award in 1993, Scott Award from The Ohio State University College of Engineering for Outstanding Academic Achievement in 2011, IEEE AP Society C-T. Tai Teaching Excellence Award in 2011, IEEE Henning Mentoring Award in 2013, IEEE Antennas and Propagation Distinguished Achievement Award in 2014, The Ohio State University Distinguished Scholar Award in 2016, The Ohio State University ElectroScience George Sinclair Award in 2017, and URSI Booker Gold Medal in 2020. His service to Professional Societies include: 2004 President of the IEEE Antennas and Propagation Society in 2004, the Chair of USNC/URSI Commission B from 2015 to 2017, the Chair of URSI Commission B (international), twice the General Chair of the IEEE Antennas and Propagation Symposium, IEEE APS Distinguished Lecturer, IEEE APS Fellows Committee Chair, IEEE-Wide Fellows Committee Member, and an Associate Editor of several journals.

Pulugurtha Markondeya Raj received the B.S. degree from the Indian Institute of Technology, Kanpur, Kanpur, India, in 1999, the M.E. degree from the Indian Institute of Science, Bangalore, India, 1995, and the Ph.D. degree from Rutgers University, Piscataway, NJ, USA, in 1999.

He is an Associate Professor with the Department of Biomedical Engineering and Electrical and Computer Engineering at Florida International University, Miami, FL, USA. He co-led several technical thrusts in electronic packaging, working with the whole electronic ecosystem, which includes semiconductor, packaging, material, tool, and end-user companies. He co-advised and mentored more than 30 graduate students, many of whom are current industry leaders and technology pioneers in the electronic packaging industry, working for Apple Inc., Texas Instruments, Intel Corp., Qualcomm, IBM, Google Inc., Broadcom, and other major electronics companies. He is widely recognized for his contributions in integrated passive components and technology roadmapping, component integration for bioelectronic, power and RF modules, and also for promoting the role of nanomaterials and nanostructures for electronics packaging applications, as evident through his several industry partnerships, invited presentations, publications and awards. His research led to 360 publications, which include ∼100 journal articles, 20 book chapters, and 16 articles in widely circulated technology magazines, ∼215 conference publications, and eight patents. His expertise is in packaging of electronic and bioelectronic systems, power-supply and wireless component integration in flex and rigid packages, and biocompatible and hermetic packaging with high-density feedthroughs.

Dr. Raj received more than 25 best-paper awards. He is an Associate Editor for IEEE TRANSACTIONS ON COMPONENTS, PACKAGING, AND MANUFACTURING TECHNOLOGY (CPMT) and *IEEE Nanotechnology Magazine*, and the Co-Chair for the IEEE Nanopackaging Technical Committee, since 2014. He served as the IEEE Distinguished Lecturer from 2020 to 2022, and the General Chair for 3-D Power Electronics Integration and Manufacturing, in 2023.